Projected Changes in Extreme Integrated Water Vapor Transport Directed Towards Switzerland in a Warming Climate

Master Thesis

Faculty of Science
University of Bern

handed in by

Samuel Ehret

2020

Supervisor:

Prof. Dr. Olivia Romppainen-Martius

Institute of Geography of the University of Bern and Oeschger Center for Climate Change Research, University of Bern

Abstract

Extreme atmospheric moisture transport directed towards Swiss topography has been linked to important flooding events in the past. The mechanism behind these moisture transport events has already been studied. Yet, no study has explored future projections for these extreme events. As such, understanding the future evolution of extreme moisture transport towards Switzerland and what may be causing it are the goals of this thesis.

This is done by using simulation carried out with the GFDL-CM3 model under the RCP8.5 climate scenario. The projected changes in extreme atmospheric integrated vapor transport (IVT) are examined using general extreme value theory, trend evolution analysis and investigation into seasonal changes. Three main regions, towards which flood triggering IVT are directed, are examined. These regions are the western, southern and eastern regions around Switzerland.

Under the RCP8.5 climate scenario, extreme IVT events will intensify for all regions over time. The main driver behind this increase is an increase of total precipitable water content in all three regions. The western region is a special case as its extreme events will happen closer to winter in the future. Thus, this region experiences an increase in wind velocity over time which drives the formation of extreme IVT in that area. Eastern and southern regions do not have any significant trend in wind speed. Sea surface temperatures in the Northwestern Mediterranean Sea are a possible driver for the increase in IVT intensity for the southern region.

Contents

1. Introduction

1.1 Motivation

September 25th 1993, Brig. It has been raining for weeks, and the past 3 days have seen record precipitation in the Saltina catchment. The Rhône river has risen and in a couple of hours tons of debris, sand and driftwood have accumulated in the center of Brig. The amount of debris has climbed up to 3 meters in some parts of town (RTS, 2015), two women have died in the rapid rise of the river and the total cost of the storm in the upper valley will amount to over 650 million Swiss Francs (Confederation, 2019).

The cause of such an event? Exceptional integrated water vapor transport (IVT) following a southeastern Potential Vorticity (PV) streamer (Froidevaux and Martius, 2016). This event is not a standalone case. Together with landslides and flood debris caused by extreme precipitation, such events have cost up to 8 billion Euros to the Swiss Confederation between 1979 and 2007 (Hilker et al., 2009). The synoptic situation of such events has been studied and understood. During the past 120 years, most major Swiss flood events were associated with synoptic structures such as Atmospheric Rivers (ARs), PV-cutoffs and PV streamers (Froidevaux and Martius, 2016; Stucki et al., 2012).

A central variable common to all of these events exists: Integrated vapor transport (IVT). This variable indicates the amount of water in a column of the atmosphere and the direction and speed at which it travels. All the synoptic situations described above can be associated with extreme IVT values in Switzerland (Froidevaux and Martius, 2016).

High IVT are not only relevant for the comprehension of extreme precipitation in Switzerland. Areas of high IVT are a fundamental component of the water cycle and while they can cause negative impacts in some regions, they are also essential for water resources in others (Dettinger et al., 2011). Furthermore, as the mean global temperature continues to rise under climate change, the water cycle will intensify. The Clausius-Clapeyron equation states that for every degree gained, the water-holding capacity of the atmosphere will increase by approximately 7%. Rising trends in global specific humidity have already been observed in the past decades (Boer, 1993; Held and

Soden, 2006; Dessler and Sherwood, 2009; Stocker et al., 2013) and are projected to continue to increase over the 21st century (Lavers et al., 2015; Stocker et al., 2013).

Most studies that attempt to understand the effect of these trends on moisture transport, focus on ARs (Espinoza et al., 2018; Ramos et al., 2015, 2016; Lavers et al., 2013; Ralph et al., 2012). These large synoptic structures are elongated stretches of water vapor located in the troposphere, and correspond to high IVT structures (Newell et al., 1992). Lavers et al. (2013) found that ARs would double in frequency over the North Atlantic by the end of the century compared to the 1980-2005 period and under the RCP8.5 scenario. Ramos et al. (2016) also described a doubling of these ARs over Europe using the same climate scenario and reference period as Lavers et al. (2013). Both studies found that higher temperatures and more important atmospheric moisture content would lead to an increase in IVT values by the end of the century. Espinoza et al. (2018) projected that ARs would decrease globally, under RCP8.5, in frequency by 10 % but that they would be more intense due to higher IVT values (+50% in the northern midlatitudes and +60% in the southern midlatitudes). The paper of Lavers et al. (2015) focused on IVT projections, again under RCP8.5, without regard to Atmospheric Rivers. This study found an increase in mean IVT values by 30-40% over the northen part of the Atlantic and Pacific. The increase in IVT values is described as being driven mainly by an increase in atmospheric moisture content.

Even if many aspects of future IVTs have been studied, there is no research about projections of flood related IVTs in Switzerland. High IVTs impacting Switzerland are typically located upstream of the country in the north eastern, southern and north western regions around Switzerland. What determines the possible impact is the angle with which they arrive in Switzerland. In fact, if an IVT arrives perpendicular to topography, it has the potential of following orographic ascent, condensating the water vapor within, and generating localized precipitation. This is how extreme precipitation events linked to IVT, such as the one affecting Brig in 1993, are generated (Froidevaux and Martius, 2016).

1.2 Study Objectives and Structure

This thesis attempts to understand how future potential flood triggering IVTs will evolve in a changing climate. It will concentrate on yearly extreme IVT values, as extreme IVTs have a higher potential of creating extreme precipitation.
Central to this work are two questions:

- What are the projected changes in IVT directed towards Swiss topography?

- What is causing the changes in moisture transport over time?

To answer these two questions, this study focuses on the output of one global circulation model (GCM), the GFDL-CM3. In a first part, the work will focus on understanding the projected trends in IVTs. In a second step, generalized extreme value (GEV) theory will be used to explore possible covariables that could help explain the projected changes in extreme IVT intensity.

This paper will be divided into seven main chapters, including this one. First a description of the data and methods used will be given in Chapters 2 and 3. Results of the study will then be presented in Chapter 4. In Chapter 5, discussion and interpretation of these results will be proposed. Finally, a conclusion will synthesize the findings of the study and an outlook for future research will be offered in Chapters 6 and 7.

2. Data

All of the data used in this work comes from the Geophysical Fluid Dynamic Laboratory - Coupled Model 3 (GFDL-CM3) model. It is a GCM developed by the National Ocean and Atmospheric Administration in association with the University of Princeton in New Jersey.

The GFDL-CM3 model is part of the Coupled Model Intercomparison Project phase 5 (CMIP5) (Taylor et al., 2011). The choice of this GCM between all the CMIP5 models, was constrained by a major factor. Not all of the CMIP5 models provide the necessary data to calculate IVT values, and the GFDL-CM3 model does. The GFDL-CM3 also has one of the highest increase in temperature over Europe by 2100, compared to other CMIP5 models (Cattiaux et al., 2013). This higher increase in temperatures makes it more likely to simulate stronger IVT signal.

The simulation spans from 1979 to 2100. From 1979 to 2005, the GCM uses historical emissions as forcing. The following years, from 2006 to 2100, all forcing scenarios used by the Intergovernmental Panel on Climate Change (IPCC) are available. The RCP8.5 scenario was used as climate scenario for the future projections. This scenario is the most "extreme" scenario used in the fifth assessment report (AR5) of the IPCC (2013) and denotes a business as usual scenario where no carbon mitigations take place over the upcoming century. The RCP8.5 scenario as future emission scenario, is likely to capture the strongest signal in IVT evolution. This is due to the fact that this scenario has the strongest increase in temperatures compared to all other IPCC scenarios (Stocker et al., 2013).

The GFDL-CM3 model simulates land, ocean, atmospheric and sea ice processes. The horizontal spatial resolution of the GCM is of 2.5° longitude by 2° latitude. It simulates 48 vertical pressure levels from approximately 1013.25 hPa to 1 Pa, thus giving insight into tropospheric, stratospheric and mesospheric processes (Donner et al., 2011).

The parameters used in this thesis are given in 6-hourly and daily time steps. The 6-hourly parameters are eastward and northward winds, specific humidity, air temperature (at 850 hPa) and surface air pressure. The daily time steps parameters are moisture in the upper portion of the soil column and sea surface temperatures.

3. Methods

3.1 Definitions

3.1.1 Vertically Integrated Water Vapor Transport

The definition of IVT follows the definition of Lavers et al. (2012):

$$IVT = \sqrt{\left(\frac{1}{g}\int_{surf.}^{top} qu\ dp\right)^2 + \left(\frac{1}{g}\int_{surf.}^{top} qv\ dp\right)^2}\ [kg\ m^{-1}\ s^{-1}] \tag{3.1}$$

In equation (3.1), g represents the gravitational constant (m/s^2), q the specific humidity (kg/kg), u and v are the zonal and meridional wind components (m/s), and p represents the pressure (Pa). The equation is integrated from the surface pressure level to the highest pressure level. For this work, the surface represents the first layer of the model ($\sim 1013.25hPa$) and the top is the upmost layer of the model ($\sim 1Pa$). IVT is given in kg/ms.

3.1.2 Total Precipitable Water

Total precipitable water (TPW) is the total amount of water in a column of the atmosphere. It is called TPW because it shows the amount of precipitation that would occur if all the water in that column would rain down. It is calculated using equation (3.2).

$$TPW = \frac{1}{g}\int_{surf}^{top} (q + q_{ice} + q_{liquid})\ dp\ [kg\ m^{-2}] \tag{3.2}$$

In equation (3.2), g is the gravitational constant (m/s^2), q is the specific humidity (kg/kg) including cloud ice (q_{ice}) and cloud water (q_{liquid}), and p represents the pressure (Pa). As for IVT (Eq: 3.1) the surface and top layer of the column, at which the column is integrated, are the surface and top layer of the GFDL-CM3 model.

3.1.3 Steering Wind

Steering Wind (SW) is a measure of the vertically averaged wind profile, weighted by the amount of water vapor transported. SW is calculated as the quotient of the IVT (Eq. 3.1) and the TPW

(Eq. 3.2).

$$SW = \frac{IVT}{TPW} \; [m \; s^{-1}] \tag{3.3}$$

3.2 Generalized Extreme Value Theory

GEV theory is central to this thesis. This subchapter serves to give a better understanding of what a GEV distribution is. As such, this section defines GEV distribution, gives an overview of the parameters in the distribution, defines "extremes" as understood in this work, explains the method used to estimate the GEV parameters, goes into linear relationship of the GEV parameters with other variables and addresses the method used to evaluate different GEV models between them.

3.2.1 Generalized Extreme Value Distribution

GEV distribution represents a distribution function for block maximas (BM) (Coles, 2011) (see section 3.2.2). This family of distribution functions is characterized by three main parameters:

- μ or the location parameter representing the center or the mean of the distribution.
- σ or the scale parameter representing the spread or the variance of the distribution.
- ξ or the shape parameter representing the end tail behavior of the distribution.

Three families of GEV distributions exist depending on the value of the shape parameter (ξ). If $\xi < 0$ the distribution is a Weibull distribution and has a finite upper bound, if $\xi > 0$ then it is a Frechet distribution with no upper limit, and if $\xi = 0$ it is a Gumbel distribution and here again the distribution is unbounded.

$$GEV(x; \mu, \sigma, \xi) = exp\left\{ - \left[1 + \xi \left(\frac{x - \mu}{\sigma} \right) \right]^{-1/\xi} \right\} \tag{3.4}$$

Equation (3.4) explains how the GEV distribution is calculated following Coles (2011) definition. x here represents the IVT BM values.

3.2.2 Defining Extremes

This thesis uses the annual BM as the definition for "extreme" events. Annual BM represents the maximum value of a variable over the course of a year. The definition as formulated by Coles (2011) is given by equation (3.5).

$$M_n = \{X_1, ..., X_n\} \tag{3.5}$$

In this equation $X_1, ..., X_n$ represents a sequence of random variables. M_n represents the maximum value in that sequence. In the case of this work, M_n will be the maximum value of IVT for

a given year.

3.2.3 Maximum Likelihood Estimation

To estimate the GEV parameters (μ, σ, ξ), the maximum likelihood estimation (MLE) technique was adopted. The MLE function allows the estimation of unknown parameters of a probability distribution or in this case of a GEV distribution (Coles, 2011).
This technique was chosen against the L-moment method on account of the advantages and shortcomings of both methods. Because of the availability of a relatively large amount of data points (n=122) and the non-stationarity of the data, the MLE estimation was considered the best alternative. This choice follows the paper of Kharin and Zwiers (2005) who found that, while being more computationally demanding, the MLE method was better suited for non-stationary data then the L-moment method.

3.2.4 Linear Relationship Between Variables and Parameters

To link parameters with the desired variables, linear models were created. This allows to estimate the importance of covariables related to IVT formation. If a linear relationship between a GEV parameter (μ, σ, ξ) and a covariable make the GEV model performed better, it would indicate a correlation between that variable and the formation of IVT BM.

The linear relationships for the location (μ) and scale (σ) parameters and the desired variable are shown in equations (3.6),(3.7) and (3.8).

$$\mu(x) = \mu_0 + \mu_1 * x \tag{3.6}$$

$$\mu(x, y) = \mu_0 + \mu_1 * x + \mu_2 * y \tag{3.7}$$

$$\sigma(x) = \sigma_0 + \sigma_1 * x \tag{3.8}$$

x and y for this thesis represent time dependent variables. To analyze the weight of these variables in the different GEV models, all covariables were standardized using equation (3.9).

$$\frac{X - \mu}{\sigma} \tag{3.9}$$

In this formula X, represents a vector of independent observations, μ is the mean of that vector and σ is the standard deviation. When applying this formula all variables correlated with the parameter of the GEV model will have a mean of 0 and a standard deviation of 1. This will allow comparison between weighted parameters for each model.

3.2.5 Bayesian Information Criterion

The Bayesian information criterion (BIC) was used to evaluate the fit between different GEV models to similar dataset. This choice of technique was made because contrary to the Akaike information criterion, BIC penalizes the model's score for each added parameter. This is useful to avoid overfitting of the GEV model by adding too many parameters. The BIC is calculated using the following formula:

$$BIC = ln(n)k - 2ln(\hat{L}) \tag{3.10}$$

In equation (3.10), n is the number of observations in the model (n = 122) and k is the number of parameters that are used in the model. The $\hat{L}$ represents the likelihood estimation and, together with the right-hand side of the equation, represents the negative log-likelihood value. The lower the BIC score, the better the model fits to the original data.

3.3 Data Selection and Processing

3.3.1 Selecting regions of interest

The first step in processing the output of the GFDL-CM3 model was the selection of grid points to analyze. The goal of these grid points is to estimate IVT values coming into the regions of interest identified by Froidevaux and Martius (2016). In their paper they used the ERA-interim reanalysis and the grid points located at 48°N, 9°E, 46°N, 9°E and 47°N, 7°E for the eastern, southern and western region respectively. Given that the GFDL-CM3 model has a lower horizontal resolution than the ERA-interim data set, it was necessary to use other grid points that could estimate the incoming IVT in each of these regions. The low topographic resolution of the GFDL-CM3 also had to be taken in account (see Fig 3.1). The selected grid points surround the smooth topographic elevation representing the Alps in the model. Froidevaux and Martius (2016) identified the angles for incoming normal IVTs (Table 3.1).

Table 3.1: Angle of advection and grid points used for each region

	Eastern region	Southern region	Western region
Advection Angle	330° – 60°	135° – 225°	270° – 360°
Grid point 1	N 49° E 8.75°	N 45° E 8.75°	N 49° E 3.75°
Grid point 2	N 49° E 11.25°	N 45° E 11.25°	N 49° E 6.25°
Grid point 3	N 47° E 8.75°	N 43° E 8.75°	N 47° E 3.75°
Grid point 4	N 47° E 11.25°	N 43° E 8.75°	N 47° E 6.25°

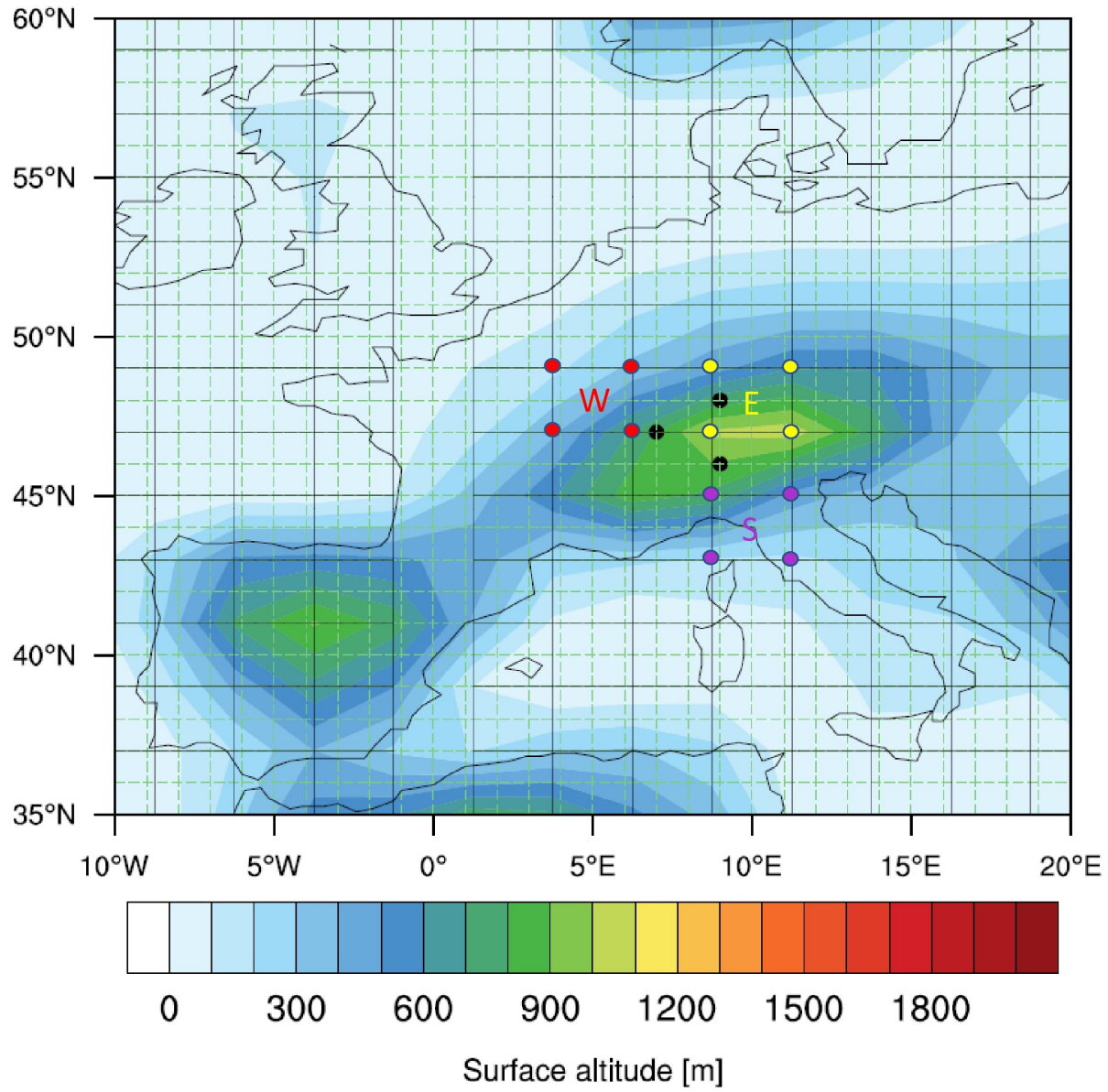

Figure 3.1: Topographic map of the GFDL-CM3 model over Europe. Lines show the ERA-interim (dotted green) and GFDL-CM3 (black) grid resolution. The 3 regions of interest (black point) are represented. The grid points selected are shown for eastern (yellow), southern (purple) and western (red) regions.

Selection of four grid points, for each region identified by Froidevaux and Martius (2016), was made. The four grid points selected per region (Fig 3.1) should capture incoming IVTs normal to the Swiss topography. The location of the four grid points for each region is indicated in table 3.1 and are illustrated in Fig 3.1.

3.3.2 Extracting Block Maxima

Annual BM values were extracted from all four grid points in each region. Amidst the four possible BMs, only the maximum value between all four grid points was retained. This process was repeated for each region. The compilation of all BM into one vector per region was done. These vectors are at the center of this study and are used for trend analysis, composite mapping and fitting of the GEV distribution (section 3.2).

3.3.3 Composite Mapping

To understand spatial structures of IVTs during BM events, composite maps were created. IVT data was extracted for the area over Europe between N 25° W 28.75° and N 69° E 33.75°. IVT values during BM events were time averaged over a past period (1979-2005) and a future period (2071-2100). The difference between these two reference periods was computed, showing the increase in IVT BM intensity over the century.

3.3.4 Extraction of Soil Moisture and Sea Surface Temperatures

Soil moisture and sea surface temperature (SST) were extracted from the GFDL-CM3 model. These variables were then used for the GEV analysis as covariables for the eastern and southern regions.
Average soil moisture over Eastern Europe was extracted during BM events in the eastern region. The area where soil moisture was extracted ranged from N 44° E 16° to N 50° E 20°.
Average SSTs over the North Western Mediterranean were extracted during BM events in the southern region. The location of extraction ranged between N 43° E 8° and N 44° E 10°.

3.4 Analysis techniques

3.4.1 Linear trend analysis

To understand the evolution of IVT BM and other variables over time, linear trend analysis was conducted. The significance was calculated using a Student t-test and the significance level was set to the 95% confidence interval. The linear models created to understand the trends in time were done using the [lm] function in R (Package: R stats). The implementation of the formula by Ross Ihaka was based on the work of Wilkinson and Rogers (1973).

3.4.2 Computation of Angular Mean Values

The time of occurrence for IVT BM events was investigated by calculating the angular means for different periods. This was done by first extracting the dates of occurrence for all IVT BM events. It was then possible to transform these dates into radiant degrees. Angular mean values can be obtained using the computed degrees and the equation (3.11).

$$angular\ mean = \arctan \frac{\frac{1}{n}\sum_{i=1}^{n} \sin(X_i)}{\frac{1}{n}\sum_{i=1}^{n} \cos(X_i)} \tag{3.11}$$

In this equation, X_i denotes a vector of angular values, $(x_1, x_2, ..., x_n)$, for a day of the year (e.g.: 1st of January = 0.01 rad, 31 of June = 3.11 rad). Once the angular mean values are calculated, it is then possible to transform the values back into days. This gives insight into the mean day of the year at which an IVT BM event is occurring.

3.4.3 Wilcoxon Signed Rank Test

The Wilcoxon signed rank test was used to evaluate statistical significance of seasonal change for IVT BM events. The test was realized between IVT occurrences for the past period (1979-2005) and the future period (2071-2100). As for the linear models (section 3.4.1), it was done using the "stats" package in R, and follows the formula developed by Wilcoxon (1945). This test is a nonparametric test that allows to determine if two samples were selected from two similar distributions. It is used as an alternative to the Student's t-test as it does not assume normality of the tested distributions.

4. Results

4.1 IVT BM Characteristic and Evolution

This section will go into the projected changes in yearly IVT BM intensity, exploring future trends of extreme IVT, the associated synoptic situations and the fundamental components of IVT. It will then investigate temperatures during IVT BM events and finally give an understanding of yearly occurrence of these events.

4.1.1 IVT BM projected Evolution

The time evolution of IVT BM in the 3 regions of advection is represented in Fig 4.1.

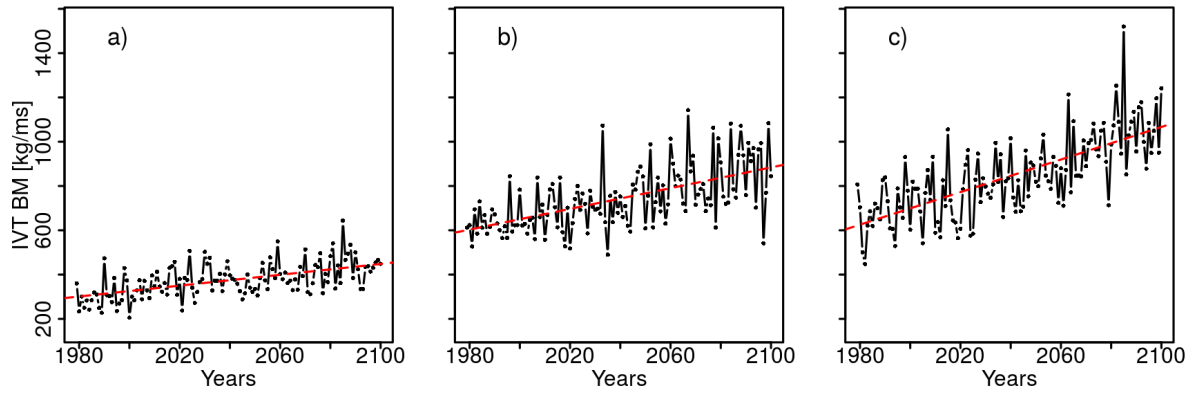

Figure 4.1: Evolution of yearly BM (black dots) over time with fitted linear trend (red dashed lines) for eastern (a), southern (b) and western (c) region.

Linear models were fitted to the yearly BM values to understand changes over time. All of the regions have a significant positive trend over time (on the 95th significance level). Nevertheless, the absolute and relative changes are not similar for all regions. The eastern region has the lowest absolute increase with an increase of 122 $kg\ m^{-1}\ s^{-1}$ and a relative increase of 37.6 % per century (Fig 4.1a). The southern region has an absolute increase of 234 $kg\ m^{-1}\ s^{-1}$ and the lowest relative increase with 36 % per century (Fig 4.1b). Finally, the western region shows

the highest increase of all three regions both in relative and absolute terms. This region has an absolute increase of 367 $kg\ m^{-1}\ s^{-1}$ and relative increase of 52.6 % per century (Fig 4.1c).

4.1.2 Composite maps

Mean IVT intensity over Europe during BM events for the three regions for historical and end of 21st century conditions is shown in Fig 4.2.

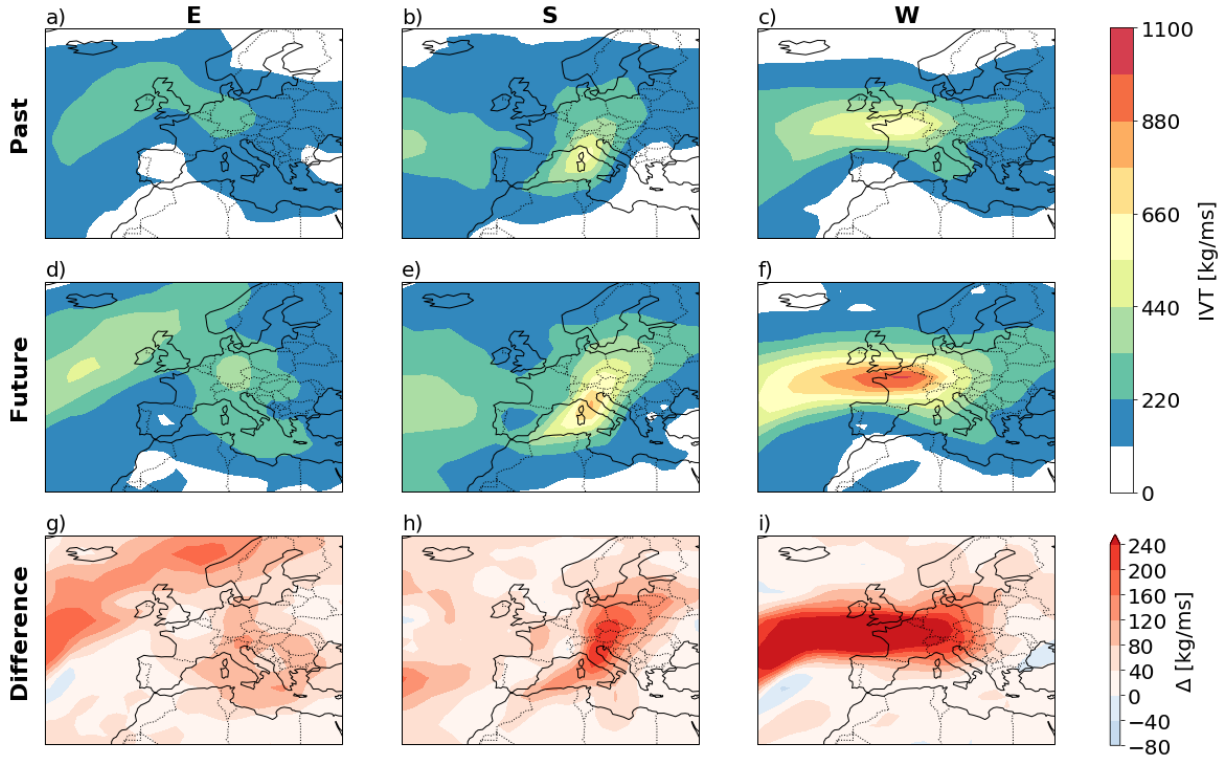

Figure 4.2: Composite maps of IVT intensity during BM events for the past period 1979-2005 (a-c), the future period 2071-2100 (d-f), and the difference between the two periods (g-i). Left panels represent eastern region, middle panels the southern region and right panels the western region.

The left panels display IVT BM changes over time for the eastern region. Historical patterns for this region are shown in Fig 4.2a. This figure indicates that high IVT values can be found in the north and eastern areas around Switzerland during BM events. The changes between this period and the future one (Fig 4.2d) are shown in Fig 4.2g. The figure displays an increase between 40 and 120 $kg\ m^{-1}\ s^{-1}$ over these same areas surrounding the eastern region.
The middle panels represent the changes for the southern region. Historical conditions (Fig 4.2b) show important IVT values south of Switzerland over the north western Mediterranean Sea and northern Italy. Fig 4.2h displays the difference between historical conditions and future conditions

(Fig 4.2e) for the southern region. Here, a strong signal for IVT intensification is presented over the north western Mediterranean Sea with an increase of 40 to 120 $kg\ m^{-1}\ s^{-1}$ and an even greater increase in northern Italy of about 200 $kg\ m^{-1}\ s^{-1}$.
The right panels show the situation for the western region. In past conditions (Fig 4.2c) high IVT values are found in northern France, southern England and in the eastern Atlantic. The evolution of these values over time are shown in Fig 4.2i. Here, again, a strong signal is simulated. IVT values increase with time over the Atlantic, France and parts of north western Europe by over 240 $kg\ m^{-1}\ s^{-1}$. The shape of the positive difference over west Europe resembles a typical AR structure.

4.1.3 Density Change in IVT BM

IVT BM in all three regions show a shift in intensity over time (Fig 4.3). The eastern region's IVT BM mean value increases by 126 $kg\ m^{-1}\ s^{-1}$ between the two reference periods. A small increase of 13 $kg\ m^{-1}\ s^{-1}$ in standard deviation occurs over time as well (Fig 4.3a).
The mean IVT BM value in the southern region rises by 208 $kg\ m^{-1}\ s^{-1}$ between past (1979-2005) and future (2071-2100) period. The distribution in this region shows a peak for the past period that transforms by the end of the century into a bimodal distribution. This change in distribution signifies a strong shift in variance and represents an increase in standard deviation of 78 $kg\ m^{-1}\ s^{-1}$ between the two reference periods (Fig 4.3b).
The western region has a large mean IVT BM value increase of 347 $kg\ m^{-1}\ s^{-1}$ between past and future period. Standard deviation also increase by 31 $kg\ m^{-1}\ s^{-1}$ in this region (Fig 4.3c).

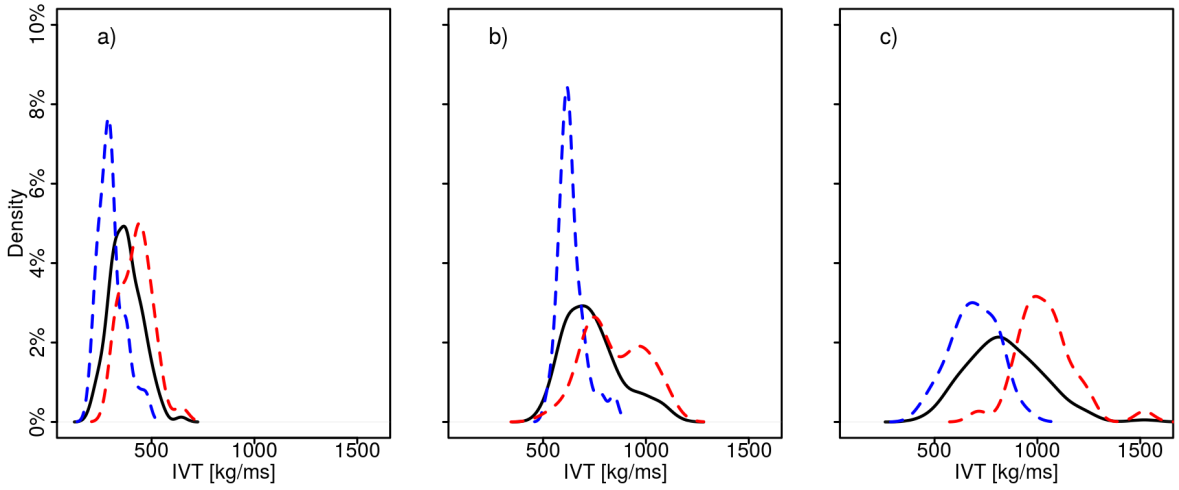

Figure 4.3: IVT BM density for eastern (a), southern (b) and western (c) region. Lines represent values for the period of 1979-2005 (blue dashed), the future period 2071-2100 (red dashed) and all 122 years of the model (black).

4.1.4 Evolution of TPW and SW

The evolution over time of the two fundamental components of IVT (total precipitable water (TPW) and steering wind (SW)) is shown in Fig 4.4 for all three regions. This figure displays TPW and SW values during the time of an IVT BM event.

The projected changes in TPW for all regions are positive and significant at a 95% significance level. The eastern and southern regions have similar significant trends with a relative centennial increase of 34% (7 $kg\ m^{-2}$) and 36% (13 $kg\ m^{-2}$) respectively (Fig 4.4 a & b). The western region has a lower but statistically significant increase with a gain of 28% (8 $kg\ m^{-2}$) per century (Fig 4.4c).
SW trends are less homogeneous between regions. The eastern region displays a decrease of -7% (- 0.8 $m\ s^{-1}$) per century (Fig 4.4d) that is not statistically significant. The southern region SW values are relatively stable with a change of only -0.32% (- 0.06 $m\ s^{-1}$), once again not statistically significant (Fig 4.4e). The only statistically significant and positive trend in SW is found in the western region. Here, SW increases by 28% (5 $m\ s^{-1}$) per century (Fig 4.4f).

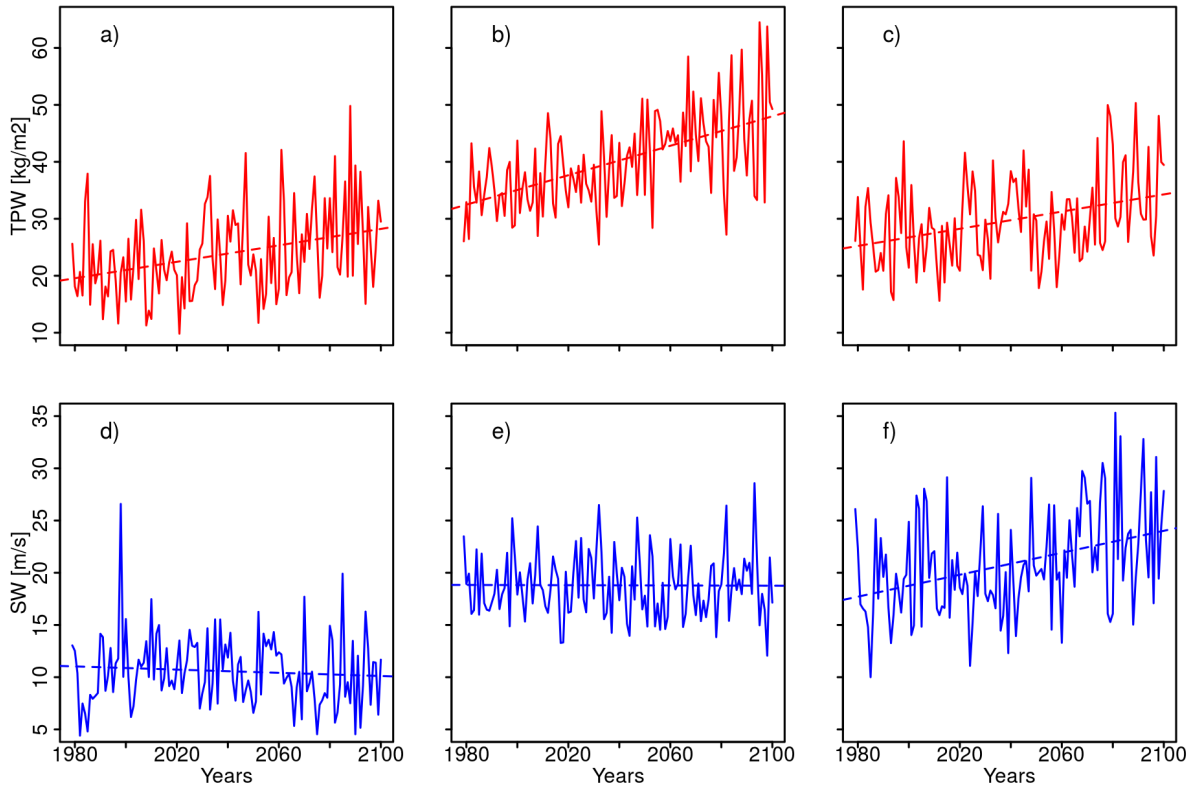

Figure 4.4: TPW (red) and SW (blue) at BM days over time. Linear trends (dashed lines) are shown for eastern (a,d), southern (b,e) and western (c,f) regions.

4.1.5 Temperatures During Events

Time series of temperatures (at 850 hPa) during IVT BM events are shown in Fig 4.5. These time series were created to understand the relative difference in TPW trends between the three regions of interest.

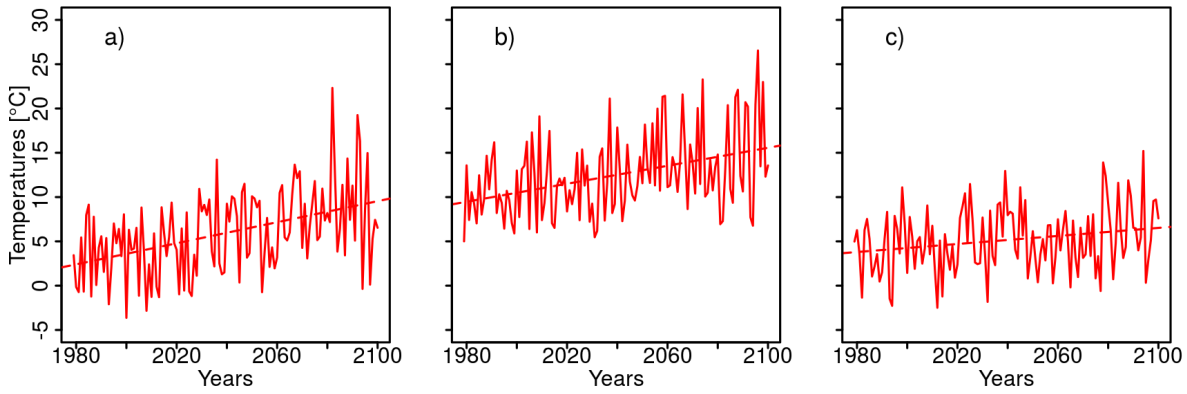

Figure 4.5: Time series of temperatures (red lines) during IVT BM event. Linear trends (red dashed lines) eastern (a), southern (b) and western (c) regions are represented.

All three regions have a significant and positive trend in temperature during IVT BM events. The eastern and southern regions have once again a similar increase in temperatures with an increase of 5.9 $°C$ and 5.1 $°C$ per century, respectively. The western region has a significant increase of 2.2 $°C$ per century.

4.1.6 Seasonality of Events

Understanding when these events happen during the year is crucial to discover the drivers behind the projected differences in temperature, TPW and SW trends between the three regions.
Figure 4.6 shows how IVT BM events are distributed over the year. During the past period (1979-2005), IVT BM events occurred in the middle of July for the eastern region, the middle of September for the southern region and towards the end of September for the western region. The Wilcoxon signed rank test was used to calculate if significant shifts in seasonality occurred between past and future periods.
The eastern region does not have a significant seasonal shift over time. The projected mean occurrence of IVT BM events for this region is only 7 days earlier in the future period.
The southern region has changes in distribution over time and its angular mean values show a minor shift towards later in the year. Events here are projected to occur 20 days later then in the past. Yet, as for the eastern region, the shift in this region is not statistically significant.
The western region is the only region that has a significant seasonal shift, with a 95 % significance

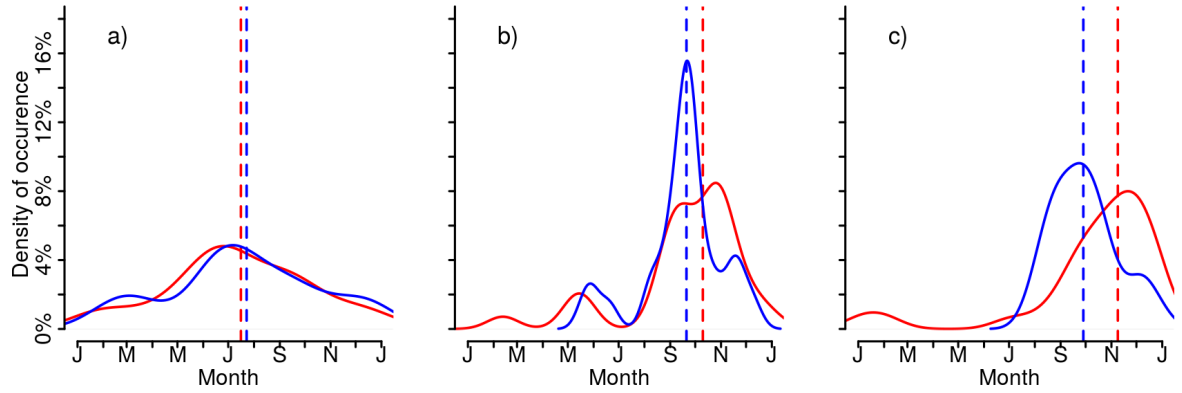

Figure 4.6: Distribution of time of occurrence for IVT BM during a year. Past period 1979-2005 (blue lines), future period 2071-2100 (red lines), and their angular mean (dashed lines) are shown for the eastern (a), southern (b) and western (c) regions.

level. This region is projected to have a seasonal shift in its IVT BM events of 42 days between the past and future periods.

4.2 GEV Analysis

In this section the results of the GEV analysis are explored. This is done by first looking at individual BIC scores for all the variables tested and then to the weighted parameters in a selection of models.

4.2.1 BIC Scores

Table 4.1 shows the different BIC scores obtained for each of the tested variables. The first row of the table shows the BIC scores for each region when no covariates are added. It serves as a benchmark to compare all other models against. This allows to understand if the model performs better or worse with the added covariate(s).

Time and temperature trends (at 850 hPa) as covariates result in similar scores because of the normalization and the fact that both increase linearly with time. The scores improve for all regions when these two variables are linked to the location parameter (μ). These models have the best scores for the eastern and western region. Temperatures (at 850 hPa) recorded during IVT BM events are also used as covariable for the location parameter (μ) and the BIC score is again better than the benchmark model.

Soil moisture in Eastern Europe was tested for the location parameter (μ) in the eastern region.

This variable was hypothesized to play a role as a water source for IVTs in the eastern region (see fig 4.2). But the model does not improve by the added variable. Sea surface temperatures in the north western Mediterranean Sea were used with the location parameter (μ) of the southern region. Again, the attempt was to understand if this region played a role as water source for extreme IVT formation in the southern region. Here, the BIC score improved by the added variable.

TPW and SW were also used as covariables for the location parameter (μ) of all three regions of interest. This allows to understand which fundamental IVT component plays the major role in the formation of extreme IVT. The TPW increases the fitting of the GEV model for all three regions. For SW, the picture is more complex, with the GEV model performing worse for the eastern region yet increasing the fitting in the southern and western regions.

TPW and SW were combined in the same model to confirm what the BIC scores indicated, but from a weighted parameter aspect. Nevertheless, when using both variables, BIC scores were improved for all three regions.

Finally, time was correlated with both location (μ) and scale (σ) parameters at the same time. Here, all scores were improved for all three regions.

Table 4.1: BIC scores for all covariables tested for each of the three regions of interest. The lower the score the better the GEV fitting to the original IVT BM data.

BIC scores for GEV Analysis	Eastern	Southern	Western
No other variables	1419	1552	1626
μ(Time or temperature trend)	1373	1520	1544
μ(Temperature during event)	1412	1546	1624
μ(Soil moisture)	1422		
μ(Sea surface temperature)		1536	
μ(Total precipitable water)	1412	1498	1615
μ(Steering wind)	1421	1544	1597
μ(TPW,SW)	1402	1138	1569
μ(Time) & σ(Time)	1378	1506	1549

4.2.2 GEV Weighted Parameters

Three models, with the overall lowest BIC score (see table 4.2) for all three regions, were extracted. What is common to all models is the negative shape parameters (ξ). This reveals that GEV distributions for IVTs are all from the Weibull distribution family. This indicates an asymptotic limit to IVT intensity.

Table 4.2: Weighted parameters for the GEV models with the overall lowest BIC scores and the benchmark model with no added variable.

Eastern						
Parameters	μ_0	μ_1	μ_2	σ_0	σ_1	ξ
No other variables	342.2			71.5		-0.15
μ(Time)	346.1	41.6		55.8		-0.08
μ(TPW,SW)	345.9	33.7	26.1	64.5		-0.16
μ(Time) & σ(Time)	346.1	42.4		55.7	2.6	-0.09
Southern						
Parameters	μ_0	μ_1	μ_2	σ_0	σ_1	ξ
No other variables	677.6			112.4		-0.006
μ(Time)	695.9	68.7		106.4		-0.15
μ(TPW,SW)	737.8	155.2	122.1	29.7		-0.65
μ(Time) & σ(Time)	696.3	65.3		103.4	30.5	-0.13
Western						
Parameters	μ_0	μ_1	μ_2	σ_0	σ_1	ξ
No other variables	767.9			164.4		-0.12
μ(Time)	789.9	127.7		114.8		-0.11
μ(TPW,SW)	783.6	73.7	102.5	122.2		-0.08
μ(Time) & σ(Time)	790.5	126.9		115.2	5.5	-0.12

Looking at the model where the location parameter (μ) is correlated with time, the amount of changes over time can be observed in the μ_1 value. The GEV models capture the same proportional changes over time as in Fig 4.1. With the highest increase in the western region, followed by the southern and then the eastern region.

When adding time as a covariate for the scale parameter (σ) as seen in the last rows of Table 4.2, changes of variance over time can be understood. These changes are quantified by the σ_1 parameter. A slight increase of variance over time takes place in both eastern and western regions. The southern region has the highest increase in variance over time. These increases in variance over time match the ones presented in section 4.1.3.

The middle row, where TPW and SW are correlated with the location parameter (μ), shows the individual importance of the two variables in the formation of extreme IVT. This is seen by the size of the μ_1 and μ_2 parameters representing TPW and SW, respectively. The μ_1 parameter is larger for the eastern and southern regions, indicating that TPW plays a major role for the formation of IVT BM in these regions. In the western region, the high value for μ_2 indicates SW as the major contributor in the formation of these extremes.

5. Discussion

5.1 IVT BM evolution and characteristics

The evolution of future IVT extremes is projected to increase significantly with time for all three regions (Fig 4.1 and Fig 4.2).

Composite analyses indicate that spatial structures of IVT in the western region are similar to AR structures. The paper of Froidevaux and Martius (2016) linked ARs to past extreme IVT events in the western region. This supports the projections from the GFDL-CM3 model, where future IVT BM events seem to follow a similar synoptic situation as described by Froidevaux and Martius (2016) (Fig 4.2).

To grasp the drivers behind this increase, IVT values have been reduced to their two fundamental components (section 4.1.4). The increase in TPW in all three regions is expected as the Clausius–Clapeyron equation describes that as temperatures rise, atmospheric humidity is expected to rise by approximately 7% per Kelvin (Boer, 1993; Held and Soden, 2006; Dessler and Sherwood, 2009; Stocker et al., 2013). It is nevertheless important to notice the magnitude of changes for each region. While the eastern and southern regions have similar relative increase in TPW (34% and 36% respectively), the western regions does not increase by the same amount (28%). Yet, as global temperatures rise, it can be expected that TPW would increase by relatively the same amount for all three regions. The western region is an outlier when looking at SW as well. This is the only region where a significant increase in SW over time is captured (see Fig 4.4).

To understand the difference in TPW between the eastern and southern regions compared to the western region, temperatures during IVT BM events must be analyzed. The time series for these temperatures capture once again the western region as an outlier. Fig 4.5 shows that the increase in temperature is not homogeneous between all three regions. The eastern region has an increase of 5.9°C per century, the southern region has a comparable increase of 5.1°C per century and the western region gains only 2.3°C per century. Thus, the difference in temperature trends could explain the differences in TPW increase between regions. As temperatures are rising less for the western region, it is to be expected to have a smaller atmospheric water increase over time as

well. Hence, explaining the lower increase in TPW for that region.

To help appreciate what is causing the differences in temperature trends the Fig 4.6 was created. This figure shows when, during the year, IVT BM events are occurring and allows an estimation of seasonal shift between past (1979-2005) and future (2071-2100) periods. The eastern region has almost no change in time of occurrence (7 days earlier) and the southern region has a small but non-significant one towards later in the year (20 days). The only statistically significant change is found in the western region. Here a shift by almost a month and a half (42 days) towards later in the year is occurring between the past period and last 30 years of the model. While IVT BM events on average happen close to the beginning of October, between 1979 and 2005, they occur on average in mid-November between 2071 and 2100.

This temporal shift explains why temperatures during events are not rising as much for the western region. As events are happening closer to winter, we can expect that the increase of temperatures would be less for that region. The seasonal trend offers an explanation for another characteristic of the western region. The SW projected trend in that region can also be related to the shift in IVT BM occurrence. Once again, as these events are happening closer to the winter period, they also occur closer to the winter cyclonic activity over Europe (Kowalewski, 2000). This winter cyclonic activity explains the increase in SW seen in the western region.

The results are in agreement with the paper of Lavers et al. (2015) that found that IVTs will increase under the RCP4.5 and RCP8.5 scenarios of the IPCC. This paper describes that the intensification in IVT values is mainly linked to low altitude specific humidity increase rather than wind velocity changes. Ramos et al. (2016) and Lavers et al. (2013) agreed on similar causes for projected IVT intensification in ARs. This is also what is found here, with close to no change in SW for the east and south regions, but an increase in TPW. In the western region, where SW increase significantly, the changes are linked to seasonal shifts, that brings these events closer to the winter cyclonic activity, rather than to a major synoptic change in wind patterns over Western Europe.

5.2 GEV Results

The GEV analysis aims to give insight into variables that could explain the formation of IVT BM. This section talks about the results gathered after performing a BIC scoring test and looks into individual weighted parameter values.

First of all, the time variable linked with the location parameter (μ) has lowered the BIC score for all regions when compared to the benchmark model (the model where no variables were cor-

related with GEV parameters). This confirms the fact that the IVT BM are non-stationary as seen in Fig 4.1. When looking at the μ_1 parameter of table 4.2 the amount of change with each passing (standardized) years can be understood. These μ_1 parameters confirm the increase in Fig 4.1 with western region having the highest increase over time, followed by the southern and finally eastern region.

Temperatures during events were correlated with the location parameter (μ) and tested for all regions. The BIC scores showed an improvement in model fitting for all regions. Yet, these improvements are smaller than when using time as a covariate. This can indicate how the Clausius–Clapeyron equation is not fully sufficient to explain all changes in IVTs over time.

When trying to correlate the location parameter (μ) of the eastern region with soil moisture over Eastern Europe, the BIC score revealed no improvement to the model. Linking this variable to the eastern region was an attempt to understand the importance of soil moisture as a water source for eastern IVTs. The lack of improvement to the model does not mean that soil moisture does not play a role in the formation of IVT in the east. Rather, it may be possible that the region and time frame selected for the extraction of soil moisture were inadequate. The region from which the variable was extracted, was estimated using the paper of Froidevaux and Martius (2016) and the composite maps of Fig 4.2. Better data selection may be needed to prove or disprove the possible role of soil moisture for the formation of IVTs for the eastern region.

For the southern region, SSTs in the north western Mediterranean were correlated with the location parameter (μ). This region was selected because it is hypothesized to be a water source for IVTs in the south of Switzerland. As for soil moisture in Eastern Europe, this region was identified using IVT value maps from Froidevaux and Martius (2016) as well as composite maps from Fig 4.2. Here the BIC scores did capture an improvement in the model indicating that there is a link between SSTs in that region and the formation of extreme IVT in southern Switzerland.

The BIC score was also calculated when using TPW or SW with the location parameter (μ). Here, the test served to understand which of the two fundamental components was the most important to the formation of IVTs for all three regions. This can be understood by looking at which of the two variables has the lowest BIC score. What these scores indicate, is that TPW is the leading factor for the increase in IVT for the eastern and southern regions. The opposite is true for the western region, where SW shows the best improvement in BIC score for that region.

The correlation of the location parameter (μ) with both TPW and SW in the same GEV model was also performed. This is to understand if the findings of the BIC scores are supported by the parameters in the models. A parameter that has a larger size can be considered to be the

most important contributor to IVT formation. The weight of the parameters μ_1 and μ_2, shown in Table 4.2, represents the weight of TPW and SW respectively. This approach confirms the results from the BIC scoring methods. TPW has more weight in the eastern and southern regions, while in the western region, SW has a higher weight. This confirms the conclusion that drivers for IVT formation in the east and south Switzerland are mainly linked to increases in TPW. It also confirms what was discussed in section 5.1, as well as the results of Lavers et al. (2015). The western region is a special case where BIC score and weighted parameter point towards SW as being the major contributor to IVT changes. This is due to the shift in time of occurrence in that region, where IVT BM event happen closer to the winter cyclonic activity over Europe.

Finally, time was linearly correlated with both location (μ) and scale (σ) parameters. This improved BIC scores compared to the benchmark model for all three regions. This improvement was even greater for the southern region, than only using time with the location parameter (μ). The captured improvement indicates that scale (σ) or variance is changing over time for all regions and that this change is especially significant for the southern region. Table 4.2 confirms this by giving values for the change in variance (σ) over time. The east and west regions increase slightly in their variance over time. The southern region has a larger increase, almost six times more than the western region and 12 times more than the eastern region.

This increase in variance over time is captured in Fig 4.3. In this figure, we can see the changes in the IVT distribution over time. The eastern region has a relatively low increase in the mean (μ) and variance (σ) over time. The western region has a significant shift in the mean (μ) as well as having a slight increase in variance (σ). The southern region also has an increase in its mean (μ), but it is when looking at the curve of the distribution that the important weight of σ_1 correlated with time becomes clear. In the past period (1979-2005), the distribution of the southern region has a peak. Later in the century (2071-2100), this peak transforms into a bimodal distribution. This change in distribution is what is captured in the GEV weighted parameters and the BIC scoring test when variance (σ) is correlated with time.

5.3 Uncertainties

Before concluding this chapter, it is necessary to discuss the shortcomings of the results at hand. There exist many sources of uncertainties in extreme value statistics related to climate data (Wehner, 2010). This section will focus on the major ones identified during this thesis and other encountered limitations.

1. *Limited GCMs*
   The first source of uncertainty, and maybe the greatest, is the number of GCMs used. Only one CMIP5 model was analyzed during this thesis. This does not allow to put in perspective

the results of the GFDL-CM3 model by comparing them to other GCM data.

2. *Block Maxima as Extremes*
   Using the BM as the definition of extreme value is very handy. It avoids the necessity of defining a threshold at which IVT can be considered as "extreme". Additionally, it allows to have only one value per year for each region, making the data easily comparable between regions. Yet, this same advantage is the main shortcoming of using BMs. BMs do not allow an appreciation of the full data at hand. Only one event per year is registered and it cannot be understood if there is an overall multiplication or reduction of these events over the course of a year.

3. *Benchmark Model*
   Another issue regarding the GEV analysis is the choice of benchmark model. Using a benchmark model with no added variable had the benefit of proving the non-stationarity of IVT BMs. But in this analysis the BIC scores are susceptible to improve with any added time dependent variables, regardless of their influence on IVT formation. Thus, it is hard to understand which variable is correlated with extreme IVT formation and which is only well correlated with time.

4. *BIC Scores*
   One of the major uncertainty in this thesis was discovered only near the very end of the project. The GEV model for the southern region shows a massive drop in BIC score when TPW and SW are both correlated to the location parameter (μ). The improvement captured is the highest of all improvements and in fact seems too high to be plausible. Looking at the quantile-quantile and probability plots of this GEV model against the original data, it appears that the model is a bad fit. This indicates a failure of the model used, which is not apparent in the BIC scoring method. The drop in BIC score comes from the maximum-likelihood estimation part of the BIC equation (see eq 3.10). There, an unexplained drop happens in the negative log-likelihood function. It is not understood why this drop occurred, but it urges caution when using the BIC score as main method to evaluate model fitting.

5. *Region Selection*
   The selection of grid point is an important source of uncertainty as well. The selected grid points shown in Fig 3.1, might be missing some of the IVTs coming into Switzerland. Changing the number of grid points analyzed per region or displacing the ones used, might prove to profoundly alter the recorded intensity of BM events.

6. Conclusions

This study attempts to understand the changes in extreme IVT for specific advection regions around Switzerland. Extreme IVTs in these areas are documented to have had an important impact on Switzerland in the form of flooding and extreme precipitation events (Froidevaux and Martius, 2016). As such, understanding the future projections of IVT values directed towards topography can serve as a first insight into Switzerland's evolving exposure to IVT related floods. The goal of this work can thus be condensated to two questions. The questions already presented in the introduction:

- What are the projected changes in IVT directed towards Swiss topography?

- What is causing the changes in moisture transport over time?

To answer these questions, the study attempts to find drivers for extreme IVT formation in these regions. It does so by looking at trends in IVT related variables, by fitting extreme values to a GEV model, and linking parameters of this model to other physical variables.

A key result is that IVTs are projected to increase for all the regions of interest. This increase is significant for all regions but is not equal between them. Mean absolute IVT values increase between past (1979-2005) and future (2071-2100) period by 126 $kg\ m^{-1}\ s^{-1}$, 208 $kg\ m^{-1}\ s^{-1}$ and 347 $kg\ m^{-1}\ s^{-1}$ for the eastern, southern and western region respectively. TPW is the main driver of these increases and it increases significantly for all three regions. SW, only has a significant change for the western region, where it increases with time. The increase in TPW is governed by the Clausius-Clapyron equation and can be linked to the increase in temperatures during IVT BM events. SW is more complex, and the projected increase in the western region seems to come from the temporal shift of these events. The western region has its IVT BM events happening closer to the winter cyclonic activity over Europe, thus explaining both the smaller increase in temperatures during events and the increase in SW for this part of Switzerland.

The GEV analysis confirmed that IVT values were not stationary over time. Using BIC values and looking at GEV parameters, it was possible to prove the increase in model efficiency when

the location parameter (μ) included time as a covariate. Soil moisture in Eastern Europe could not be proven to play a role in IVT formation in the eastern region. SSTs in the north-western Mediterranean was shown to improve the GEV model for the southern region. TPW and SW importance for IVT formation have both been analyzed using BIC scoring and weighted parameters. This has shown the relevance of TPW in IVT formation in the eastern and southern regions. In return, the changes in IVT in the western region are mostly influenced by the increasing SWs. Variance in IVT intensity has increased for all regions. This is especially true for the southern region where the trend in the scale parameter (σ_1), when link to time, shows a high value compared to the two other regions.

With this information at hand, it is then possible to answers our two central questions.

What are the projected changes in IVT directed towards Swiss topography?
IVT BM will increase for all regions of Switzerland. GEV analysis demonstrates that future IVT BM values are non-stationary. Additionally, time-series and density plots show an increase in IVT BM values over time.

What is causing the changes in moisture transport over time?
The increase in water vapor in the atmosphere is the main driver of IVT BM increase. TPW is projected to increase for all regions and drives higher IVT values over time. This increase is closely linked to temperature changes over time. SW only plays a role for the western region, where events happen closer to winter. Composite analysis do not indicate important shift in IVT BM synoptic structure over time. The increase in TPW in the southern region could be related to an increase in SST in the Northwestern Mediterranean. Finally, it is unlikely that soil moisture is a significant contributor to IVT formation in the east.

7. Outlook

This closing chapter addresses some of the limitations encountered in the thesis and gives some insight into future research opportunities.

7.1 Further Research Opportunities

1. *More GCMs to be tested*
   CMIP5 has multiple GCMs that can provide projections for future IVTs. A first step in deepening this research would be to repeat the analysis made using the GFDL-CM3 model with other models. The two first models to be tested would be the GFDL-ESM2G and CNRM-CM5 models as they both have enough vertical levels to calculate IVTs.

2. *Changing the Benchmark for GEV Analysis*
   To overcome one of the limitations of this work, it would be necessary to change the benchmark model used in the GEV analysis. In this study, any GEV model that is correlated with a time dependent variable has a good chance of lowering the BIC score compared to the current benchmark model score. This is due to the non-stationarity of IVT BM over time. This could be avoided by using as benchmark the GEV model where the location parameter (μ) is correlated with time. This would allow it to take in account the non-stationarity of the data and would make it harder to have a lower BIC score than the benchmark model. If an added variable lowers the BIC score under the new benchmark model, it would be easier to confirm its relevance in the formation of extreme IVTs.

3. *SSTs in the North Atlantic*
   In the attempt of finding a water source for IVTs in the western region, it would be interesting to look at SSTs in the North Atlantic Ocean. As shown in Fig 4.2 high IVT reaching the western region extend from the North Atlantic to Western Switzerland. As such, a strong link between western IVTs and SSTs in that region might be found when using the variable in the GEV analysis.

4. *Drivers for SW Trends*
   As the western region is the only region that has an increase in SW, it would be compelling

to understand some of the processes creating these increase. Linking, for example, the Arctic Oscillation with the IVT formation in the west, could give insight into drivers for SW trends.

5. *Non-linear Relationships*
   All relationships created between variables and GEV parameters were made using linear models. Yet, it is not necessarily the case that these relations should be linear. It could be imagined that a logarithmic relationship between time and the location (μ) and scale (σ) parameters would be more precise. These types of relationships should also be explored and compared to a new benchmark model.

6. *Using r-Largest Order*
   To address the shortcomings of using BM as "extremes", one could turn to the r-largest order statistics. This allows to record r numbers of BM per year (Coles, 2011) and has been used in previous studies (Soares and Scotto, 2004). This enables a more precise understanding of the evolution of extreme IVTs in a transient climate.

Bibliography

Boer, G. J. (1993). Climate change and the regulation of the surface moisture and energy budgets. *Climate Dynamics*, 8(5):225–239.

Cattiaux, J., Douville, H., and Peings, Y. (2013). European temperatures in CMIP5: origins of present-day biases and future uncertainties. *Climate Dynamics*, 41(11):2889–2907.

Coles, S. (2011). *An introduction to statistical modeling of extreme values*. Springer, London. OCLC: 751837244.

Confederation, S. (2019). Plate-forme nationale « Dangers naturels » PLANAT– plate-forme d'information pour gérer les dangers naturels en Suisse [Images Détails]. http://www.planat.ch/fr/images-details/datum/2011/06/09/hochwasser-brig-1993/. Accessed: 2019-10-29.

Dessler, A. E. and Sherwood, S. C. (2009). A Matter of Humidity. *Science*, 323(5917):1020–1021.

Dettinger, M. D., Ralph, F. M., Das, T., Neiman, P. J., and Cayan, D. R. (2011). Atmospheric Rivers, Floods and the Water Resources of California. *Water*, 3(2):445–478.

Donner, L. J., Wyman, B. L., Hemler, R. S., Horowitz, L. W., Ming, Y., Zhao, M., Golaz, J.-C., Ginoux, P., Lin, S.-J., Schwarzkopf, M. D., Austin, J., Alaka, G., Cooke, W. F., Delworth, T. L., Freidenreich, S. M., Gordon, C. T., Griffies, S. M., Held, I. M., Hurlin, W. J., Klein, S. A., Knutson, T. R., Langenhorst, A. R., Lee, H.-C., Lin, Y., Magi, B. I., Malyshev, S. L., Milly, P. C. D., Naik, V., Nath, M. J., Pincus, R., Ploshay, J. J., Ramaswamy, V., Seman, C. J., Shevliakova, E., Sirutis, J. J., Stern, W. F., Stouffer, R. J., Wilson, R. J., Winton, M., Wittenberg, A. T., and Zeng, F. (2011). The Dynamical Core, Physical Parameterizations, and Basic Simulation Characteristics of the Atmospheric Component AM3 of the GFDL Global Coupled Model CM3. *Journal of Climate*, 24(13):3484–3519.

Espinoza, V., Waliser, D. E., Guan, B., Lavers, D. A., and Ralph, F. M. (2018). Global Analysis of Climate Change Projection Effects on Atmospheric Rivers. *Geophysical Research Letters*, 45(9):4299–4308.

Froidevaux, P. and Martius, O. (2016). Exceptional integrated vapour transport toward orography: an important precursor to severe floods in Switzerland: Integrated Vapour Transport and Floods in Switzerland. *Quarterly Journal of the Royal Meteorological Society*, 142(698):1997–2012.

Held, I. M. and Soden, B. J. (2006). Robust Responses of the Hydrological Cycle to Global Warming. *Journal of Climate*, 19(21):5686–5699.

Hilker, N., Badoux, A., and Hegg, C. (2009). The Swiss flood and landslide damage database 1972–2007. *Natural Hazards and Earth System Sciences*, 9(3):913–925.

Kharin, V. V. and Zwiers, F. W. (2005). Estimating Extremes in Transient Climate Change Simulations. *Journal of Climate*, 18(8):1156–1173.

Kowalewski, M. (2000). The winter routes of cyclones over europe. *Miscellanea Geographica*, 9:29–38.

Lavers, D. A., Allan, R. P., Villarini, G., Lloyd-Hughes, B., Brayshaw, D. J., and Wade, A. J. (2013). Future changes in atmospheric rivers and their implications for winter flooding in Britain. *Environmental Research Letters*, 8(3):034010.

Lavers, D. A., Ralph, F. M., Waliser, D. E., Gershunov, A., and Dettinger, M. D. (2015). Climate change intensification of horizontal water vapor transport in CMIP5. *Geophysical Research Letters*, 42(13):5617–5625.

Lavers, D. A., Villarini, G., Allan, R. P., Wood, E. F., and Wade, A. J. (2012). The detection of atmospheric rivers in atmospheric reanalyses and their links to British winter floods and the large-scale climatic circulation. *Journal of Geophysical Research: Atmospheres*, 117(D20).

Newell, R. E., Newell, N. E., Zhu, Y., and Scott, C. (1992). Tropospheric rivers? – A pilot study. *Geophysical Research Letters*, 19(24):2401–2404.

Ralph, F. M., Coleman, T., Neiman, P. J., Zamora, R. J., and Dettinger, M. D. (2012). Observed Impacts of Duration and Seasonality of Atmospheric-River Landfalls on Soil Moisture and Runoff in Coastal Northern California. *Journal of Hydrometeorology*, 14(2):443–459.

Ramos, A. M., Tomé, R., Trigo, R. M., Liberato, M. L., and Pinto, J. G. (2016). Projected changes in atmospheric rivers affecting europe in cmip5 models. *Geophysical Research Letters*, 43(17):9315–9323.

Ramos, A. M., Trigo, R. M., Liberato, M. L. R., and Tomé, R. (2015). Daily Precipitation Extreme Events in the Iberian Peninsula and Its Association with Atmospheric Rivers. *Journal of Hydrometeorology*, 16(2):579–597.

RTS (2015). Brigue sous l'eau. https://www.rts.ch/archives/tv/information/telejournal/5854662-brigue-sous-l-eau.html. Accessed: 2019-10-29.

Soares, C. G. and Scotto, M. (2004). Application of the r largest-order statistics for long-term predictions of significant wave height. *Coastal Engineering*, 51(5-6):387–394.

Stocker, T. F., Qin, D., Plattner, G.-K., Tignor, M., Allen, S. K., Boschung, J., Nauels, A., Xia, Y., Bex, V., Midgley, P. M., et al. (2013). Climate change 2013: The physical science basis.

Stucki, P., Rickli, R., Brönnimann, S., Martius, O., Wanner, H., Grebner, D., and Luterbacher, J. (2012). Weather patterns and hydro-climatological precursors of extreme floods in Switzerland since 1868. *Meteorologische Zeitschrift*, 21(6):531–550.

Taylor, K. E., Stouffer, R. J., and Meehl, G. A. (2011). An Overview of CMIP5 and the Experiment Design. *Bulletin of the American Meteorological Society*, 93(4):485–498.

Wehner, M. (2010). Sources of uncertainty in the extreme value statistics of climate data. *Extremes*, 13(2):205–217.

Wilcoxon, F. (1945). Individual comparisons by ranking methods. biom bull 1: 80–83.

Wilkinson, G. N. and Rogers, C. E. (1973). Symbolic Description of Factorial Models for Analysis of Variance. *Journal of the Royal Statistical Society. Series C (Applied Statistics)*, 22(3):392–399.

List of Figures

List of Tables

8. Acknowledgments

Many people have supported this master thesis and have helped in producing many key aspects of this work. It would not have been possible to finish this project without their help.
First, I would like to extend my gratitude to my supervisor Prof. Dr. Olivia Romppainen-Martius for supervising this thesis, supporting me in my research and helping me in key decision making moments.
I am very thankful to have had the opportunity to work under the supervision of my advisor Regula Mülchi. I thank her for her patience in answering all my questions and her support and interest from day one of this work.
Acknowledgments have to be made to Dr. Timothy Raupach, Dr. Andrey Martynov, Pauline Rivoire and Mubashshir Ali who gave me significant help and guidance in Shell, Linux, Python and statistical analysis. Without their collaboration many analyses would have been impossible to conduct.
I would like to extend my appreciations to the rest of the climate impact group as well as the climatology group. Many people in these groups have given important insight and feedback to this work. This thesis has gained in quality because of inputs from their many areas of expertise.
I am thankful towards Eléonore Perret, who had the arduous task of proofreading this work many times. It would have been impossible to give back a corrected version of this thesis without her constant contribution.
I must thank all the R package developers for sharing the user-friendly packages with the scientific community.
Finally, I want to honor my family and friends for their important encouragement, support and love.

Declaration of consent

on the basis of Article 30 of the RSL Phil.-nat. 18

Last, first name:	Ehret Samuel
Registration number:	13-413-240
Study program:	M.Sc. in Climate Sciences Bachelor ☐ Master ☒ Dissertation ☐
Title of the thesis:	Projected Changes in Extreme Integrated Water Vapor Transport Directed Towards Switzerland in a Warming Climate
Supervisors:	Prof. Dr. Olivia Romppainen-Martius

I declare herewith that this thesis is my own work and that I have not used any sources other than those stated. I have indicated the adoption of quotations as well as thoughts taken from other authors as such in the thesis. I am aware that the Senate pursuant to Article 36 paragraph 1 litera r of the University Act of 5 September, 1996 is authorized to revoke the title awarded on the basis of this thesis.
For the purposes of evaluation and verification of compliance with the declaration of originality and the regulations governing plagiarism, I hereby grant the University of Bern the right to process my personal data and to perform the acts of use this requires, in particular, to reproduce the written thesis and to store it permanently in a database, and to use said database, or to make said database available, to enable comparison with future theses submitted by others.

Bern, February 5, 2020